

Noise generation by a vortex ring near porous and elastic edges

Huansheng Chen* and Justin W. Jaworski † Lehigh University, Bethlehem, Pennsylvania, 18015

The noise generated by a porous or elastic edge is investigated analytically using a vortex ring source in a quiescent fluid. Use of a vortex ring on a rectilinear path near an edge permits the investigation of scaling behaviors for the radiated acoustic power that are analogous to those derived for turbulence edge noise using the Wiener-Hopf technique. A solution methodology based on Green's functions solves for the scattered acoustic field and identifies parametric groups to test the theoretical sixth- and seventh-power dependencies on the vortex ring speed for the sound radiated by porous or elastic edges, respectively. The vortex-ring configuration in a quiescent fluid is pursued to minimize the risk of corruption of the weak noise signal from an elastic edge by secondary noise sources present in aeroacoustic wind tunnels.

I. Introduction

The seminal analysis of Lighthill [1] determined that a free-field turbulent eddy may be modeled as an acoustically-compact quadrupole source for flows with a small characteristic Mach number. A compact turbulence source radiates sound with an intensity proportional to U^3M^5 or U^8 , where U and M are the characteristic flow speed and the Mach number, respectively. This famous 'eighth-power law' is modified when the turbulence source is near a solid surface. For example, the acoustic efficiency increases by a factor of M^{-2} (i.e., the acoustic power scales as $\Pi \sim U^6$) for acoustically-compact bodies [2] and by M^{-3} (i.e., $\Pi \sim U^5$) for turbulent eddies that are within an acoustic wavelength of an edge [3, 4]. The directivity of the radiated sound changes accordingly with the acoustic power dependence on flow speed, where a dipolar acoustic field for the U^6 scaling becomes a cardioid for U^5 behavior [3–5].

The efficient conversion of the energy in turbulence sources into radiated sound by rigid edges has continued to motivate research into creative means to reduce leading- and trailing-edge noise in the aerospace community. One candidate passive noise mitigation strategy is to make the edge compliant, whereby the interaction of the edge with a turbulent eddy generated in the wing boundary layer is relaxed. Howe [6] carried out a Wiener-Hopf analysis to investigate turbulence scattering by a semi-infinite elastic edge, which was extended by Jaworski and Peake [7] to poroelastic edges. The latter work identified a new parametric regime where the acoustic power from elastic edges would scale with the seventh power of the flow speed, i.e. $\Pi \sim U^7$, a factor of only M^{-1} stronger than a free-field quadrupole. However, experimental confirmation of this scaling for elastic edges is not likely possible with conventional aeroacoustic facilities, where secondary noise sources such as roughness noise [8–10] are likely to dominate the elastic edge noise emission.

To circumvent this experimental limitation, an alternative approach using a moving vortex source is proposed to inform an experimental campaign to test the U^7 scaling. This approach stems from the analysis by Crighton [11] for a line vortex passing round a half plane, which recovers the fifth-power velocity scaling determined earlier by Green's function [3] and Wiener-Hopf [4] analyses of turbulence noise scattering. Kambe $et\ al$. [12] employed the low-frequency Green's function for a rigid half-plane developed by Howe [13] to confirm the U^5 scaling of noise generated by sending a vortex ring on a rectilinear path near the edge of the half plane. Crucially, the vortex ring configuration of Kambe $et\ al$. does not utilize a mean flow and therefore does not introduce the complication of creating secondary noise sources that would corrupt a wind tunnel measurement.

The present work adapts the works of Kambe *et al.* [12] and Jaworski and Peake [7] to develop a vortex-ring analogue to the poroelastic-edge noise problem. Special attention is paid to the limiting cases of porous-rigid and elastic-impermeable plate conditions. This work seeks to identify parametric ranges for the design and testing of a vortex-ring experimental apparatus to examine the validity of the U^7 acoustic scaling prediction of Jaworski and Peake [7]. The remainder of this paper is organized in the following manner. Section II outlines the mathematical framework based on Green's functions to produce separate estimates for the acoustic field emitted from a vortex ring passing near porous or elastic edges, where the Kambe *et al.* [12] results for a rigid edge furnish a parametric check on these analyses. Sections III and IV summarizes the main results from this study and presents concluding remarks.

^{*}Ph.D. Student, Department of Mechanical and Mechanics, Student Member AIAA

[†]Assistant Professor, Department of Mechanical and Mechanics, Senior Member AIAA

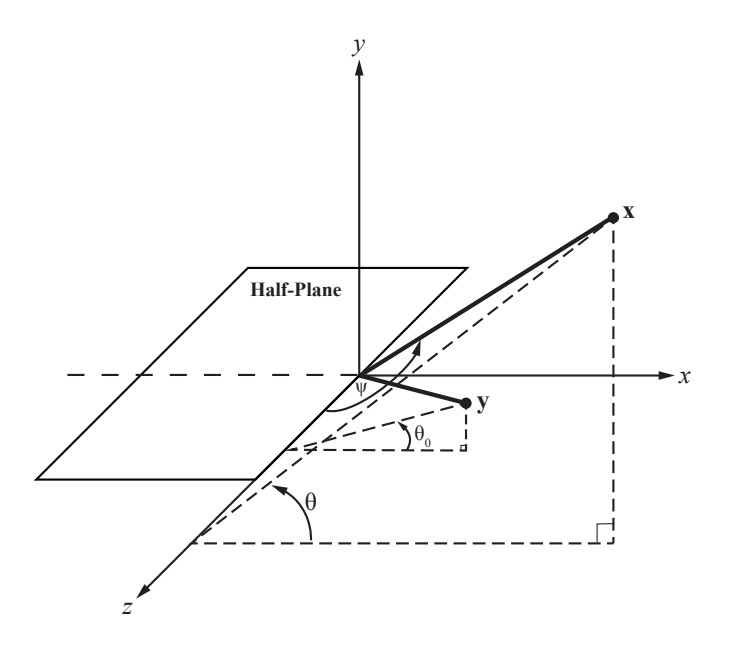


Fig. 1 Schematic of the half-plane (x < 0, y = 0) and the positions of point source y and observer x

II. Mathematical Formulation

A. Equation of vortex sound

Aerodynamic sound generated by low Mach number turbulence of uniform mean density is governed by the inhomogeneous wave equation [14]

$$\left(\frac{1}{c^2}\frac{\partial^2}{\partial t^2} - \nabla^2\right) p = \rho_0 \operatorname{div}(\boldsymbol{\omega} \wedge \boldsymbol{v}),\tag{1}$$

which admits the solution

$$p(\mathbf{x},t) = -\rho_0 \int \int (\omega \wedge \mathbf{v})(\mathbf{y},\tau) \cdot \frac{\partial G(\mathbf{x},\mathbf{y};t-\tau)}{\partial \mathbf{y}} \,\mathrm{d}\mathbf{y} \,\mathrm{d}\tau, \qquad (2)$$

where p is the acoustic pressure, ρ_0 is the mean fluid density, c is the isentropic speed of sound. ω is the vorticity distribution in an ideal fluid neglecting viscous dissipation, v is the vorticity convection velocity, and $G(x, y; t - \tau)$ is the time-domain Green's function.

Following the procedure of Kambe *et al.* [12] by introducing a gradient Green's function by the relation $\partial G(x, y; t - \tau)/\partial y$ with the condition $\partial G/\partial n = 0$ for y on the boundary surface S, we find an alternative expression for the pressure in Eq. (2):

$$p(\mathbf{x},t) = \rho_0 \frac{\partial}{\partial t} \int \int \mathbf{G}(\mathbf{x}, \mathbf{y}; t - \tau) \cdot \boldsymbol{\omega}(\mathbf{y}, \tau) \, \mathrm{d}\mathbf{y} \, \mathrm{d}\tau,$$
 (3)

At sufficiently small Mach numbers, $G(x, y; t - \tau)$ may be approximated by the compact Green's function, which is described further in the following sections.

B. Green's function for a semi-infinite plate

The present work studies the acoustic emission by a vortex ring moving near the edge of semi-infinite thin porous or elastic plate that lies in the region $-\infty < x < 0$, y = 0, $-\infty < z < \infty$ of the rectangular coordinate system (x, y, z), as shown in Fig. 1. To determine the expression of pressure p(x, t) in Eq. (2), the corresponding Green's functions for different plate properties must be determined.

Suppose a Green's function that be definition produces the solution at a distant point $\mathbf{x} = (x_1, x_2, x_3)$ that results from an impulsive point source of unit strength at position $\mathbf{y} = (y_1, y_2, y_3)$ near the edge of a semi-infinite porous or elastic plate. The Green's function also must exhibit outgoing wave behavior and satisfy [14]

$$\left(\frac{1}{c^2}\frac{\partial^2}{\partial t^2} - \nabla^2\right)G(x, y; t - \tau) = \delta(x - y)\delta(t - \tau),\tag{4}$$

where the right hand side represents the impulsive point source that vanishes except at $t = \tau$. By the reciprocal theorem [15], the positions of source y and observer x may be interchanged, and we may solve for the sound field observed at a near point y due to a monopole source at a distant point x. The problem thus reduces to the solution for the Green's function G as a function of observer positions y close to the edge, where is a diffraction problem that can be solved in the manner described, for example, by Crighton and Leppington [4] or Jaworski and Peake [7]. It is shown that near the edge of the plate that

$$G = G_0 + G_s, (5)$$

where G_0 and G_s are the time-domain velocity potentials for the incident field and the scattered field, respectively. The time-domain Green's function G is related to its Fourier transform \widehat{G} by

$$G(\mathbf{x}, \mathbf{y}; t) = \frac{1}{2\pi} \int_{-\infty}^{+\infty} \widehat{G}(\mathbf{x}, \mathbf{y}; k) e^{-i\omega t} d\omega, \tag{6}$$

where $k = \omega/c$ is the wavenumber and ω is the angular frequency.

It is convenient to decompose \widehat{G} into the sum $\widehat{G} = \widehat{G_0} + \widehat{G_s}$, and the expressions of $\widehat{G_0}$ and $\widehat{G_s}$ are given in the Appendix for different plate properties. Following the procedure by Kambe *et al.* [12], we apply the Fourier inversion formula in Eq. (6), and the time-domain Green's function for the incident field can be obtained in the series form

$$G_0(\mathbf{x}, \mathbf{y}; t) = \frac{1}{4\pi x} \left(\delta(t_r) + \frac{\mathbf{x} \cdot \mathbf{y}}{cx} D_t \delta(t_r) + \frac{(\mathbf{x} \cdot \mathbf{y})^2}{2c^2 x^2} D_t^2 \delta(t_r) + \ldots \right), \tag{7}$$

where x = |x| and

$$D_t^m \delta(t) = \frac{1}{2\pi} \int_{-\infty}^{+\infty} (-i\omega)^m e^{-i\omega t} d\omega, \quad D_t = \frac{\partial}{\partial t}, \quad t_r = t - \frac{x}{c}.$$
 (8)

If G_0 in Eq. (7) is substituted in Eq. (2), the first term contributes nothing to the sound field since it does not include y, and the contribution from the second term of G_0 is also zero due to the vanishing integral around the half-plane surface. Therefore the total Green's function $G = G_0 + G_s$ may be approximated to leading order by G_s only, provided that the third term of G_0 remains subdominant.

The Green's function in time domain for the scattered solution in the acoustic far field will be discussed for two cases: porous-rigid and impermeable-elastic edges.

1. Porous-rigid case

Substitute Eq. (56) in Appendix. A into into Eq. (7) gives, after integration,

$$G_s(\mathbf{x}, \mathbf{y}; t) = \frac{1}{2\pi^{\frac{3}{2}}c} \Phi_{\frac{1}{2}}(Y) \frac{\sin \theta_0 \sin \psi_0}{\mu^{\frac{1}{2}}x} D_t \delta(t_*), \tag{9}$$

where $\Phi_{\frac{1}{2}}(Y) = Y^{\frac{1}{2}} \sin \frac{\theta}{2}$ corresponds to the velocity potential of a hypothetical irrotational flow around the edge, $t_* = t - |x - y_3 k|/c$, k = (0,0,1), and $\mu = \alpha_H \overline{K}_R/R$ is a parameter determining the porous effects. Specifically, α_H is the open area fraction of the the surface with pores of nominal radius R, and $\overline{K}_R = 2K_R/(\pi R)$, where K_R is the Rayleigh conductivity of the pore [7].

It is observed that $G_s(x, y; t)$ is dominant to the third term of G_0 in Eq. (7) as $x \to \infty$ in the far field. Therefore, the total field $G_{rp} = G_0 + G_s$ for the highly porous-rigid ($\mu/k \gg 1$, as indicated in the Appendix) case can be approximated by G_s in Eq. (9), i.e. $G_{rp} \approx G_s$. This form of Green's function obviates that $\partial G/\partial y_3$ is subdominant to the magnitudes

of the derivatives in other two directions, i.e., $\partial G/\partial y_1$ and $\partial G/\partial y_2$. Therefore, $\partial G(x, y; t)/\partial y$ can be approximated by the two-dimensional vector,

$$\frac{\partial G(x,y;t)}{\partial y} = \left(\frac{\partial}{\partial y_1} \Phi_{\frac{1}{2}}(Y), \frac{\partial}{\partial y_2} \Phi_{\frac{1}{2}}(Y), 0\right) \frac{1}{2\pi^{\frac{3}{2}}c} \frac{\sin\theta_0 \sin\psi_0}{\mu^{\frac{1}{2}}x} D_t \delta(t_*). \tag{10}$$

Equation (10) may be reworked into a more useful form by introducing a stream function $\Psi_{\frac{1}{2}}(Y)$ corresponding to the potential flow $\Phi_{\frac{1}{4}}(Y)$,

$$\Psi_{\frac{1}{2}}(Y) = -Y^{\frac{1}{2}}\cos\frac{\theta}{2},\tag{11}$$

which satisfies the Cauchy-Riemann equations,

$$\frac{\partial}{\partial y_1} \Phi_{\frac{1}{2}}(Y) = \frac{\partial}{\partial y_2} \Psi_{\frac{1}{2}}(Y), \quad \frac{\partial}{\partial y_2} \Phi_{\frac{1}{2}}(Y) = -\frac{\partial}{\partial y_1} \Psi_{\frac{1}{2}}(Y). \tag{12}$$

Therefore, Eq. (10) can be rewritten as

$$\frac{\partial G(\mathbf{x}, \mathbf{y}; t)}{\partial \mathbf{y}} = \frac{\partial}{\partial \mathbf{y}} \times [\Psi_{\frac{1}{2}}(\mathbf{Y}) \mathbf{k}] \frac{1}{2\pi^{\frac{3}{2}} c} \frac{\sin \theta_0 \sin \psi_0}{\mu^{\frac{1}{2}} x} D_t \delta(t_*)$$
(13)

Substitute Eq. (13) into Eq. (2) and apply the dynamic equation for the vorticity of the vortex ring,

$$\frac{\partial \boldsymbol{\omega}}{\partial t} + \nabla \times (\boldsymbol{\omega} \wedge \boldsymbol{v}) = 0, \tag{14}$$

the final expression of the acoustic pressure in the far field can be represented by,

$$p_{rp}(\mathbf{x},t) = \rho_0 D_t \int \int \omega_3(\mathbf{y},\tau) F(\mathbf{x},\mathbf{Y}) D_t \delta(t_* - \tau) d\mathbf{y} d\tau,$$

$$= \rho_0 D_t^2 \int \omega_3(\mathbf{y},t_r) F(\mathbf{x},\mathbf{Y}) d\mathbf{y},$$
(15)

where

$$F(x, Y) = \frac{1}{2\pi^{\frac{3}{2}}c} \frac{\sin \theta_0 \sin \psi_0}{\mu^{\frac{1}{2}}x} \Psi_{\frac{1}{2}}(Y). \tag{16}$$

Note that t_* is replaced by $t_r = t - x/c$ in Eq. (15) in the limit $x \to \infty$ for a compact source.

2. Impermeable-elastic case

Similarly, the Green's function for the acoustic field scattered by the elastic edge in time domain can be obtained by substituting Eq. (58) into Eq. (7),

$$G_s(\mathbf{x}, \mathbf{y}; t) = \frac{i}{2\pi^{\frac{3}{2}} c^{\frac{3}{2}}} \Phi_{\frac{1}{2}}(\mathbf{Y}) \frac{\sin \theta_0 \sin \psi_0}{\epsilon^{\frac{1}{2}} x} D_t^{\frac{3}{2}} \delta(t_*), \tag{17}$$

This result is valid in the asymptotic limit $k\epsilon^{-1/2} \ll 1$, where ϵ is the intrinsic fluid loading parameter [7, 14, 16] that depends only on the properties of the structure and fluid. By inspection, the total field $G_e = G_0 + G_s$ for the impermeable-elastic case can also be approximated by G_s in Eq. (17):

$$G_e(\mathbf{x}, \mathbf{y}; t) = \frac{i}{2\pi^{\frac{3}{2}} c^{\frac{3}{2}}} \Phi_{\frac{1}{2}}(Y) \frac{\sin \theta_0 \sin \psi_0}{\epsilon^{\frac{1}{2}} x} D_t^{\frac{3}{2}} \delta(t_*), \tag{18}$$

such that the pressure observed in the acoustic far field is

$$p_{e}(\mathbf{x},t) = \rho_{0}D_{t} \int \int \omega_{3}(\mathbf{y},\tau)F(\mathbf{x},\mathbf{Y})D_{t}^{\frac{3}{2}}\delta(t_{*}-\tau)\mathrm{d}\mathbf{y}\mathrm{d}\tau$$
$$= \rho_{0}D_{t}^{\frac{5}{2}} \int \omega_{3}(\mathbf{y},t_{r})F(\mathbf{x},\mathbf{Y})\mathrm{d}\mathbf{y}. \tag{19}$$

where

$$F(x,Y) = \frac{i}{2\pi^{\frac{3}{2}}c^{\frac{3}{2}}} \frac{\sin\theta_0 \sin\psi_0}{\epsilon^{\frac{1}{2}}x} \Psi_{\frac{1}{2}}(Y). \tag{20}$$

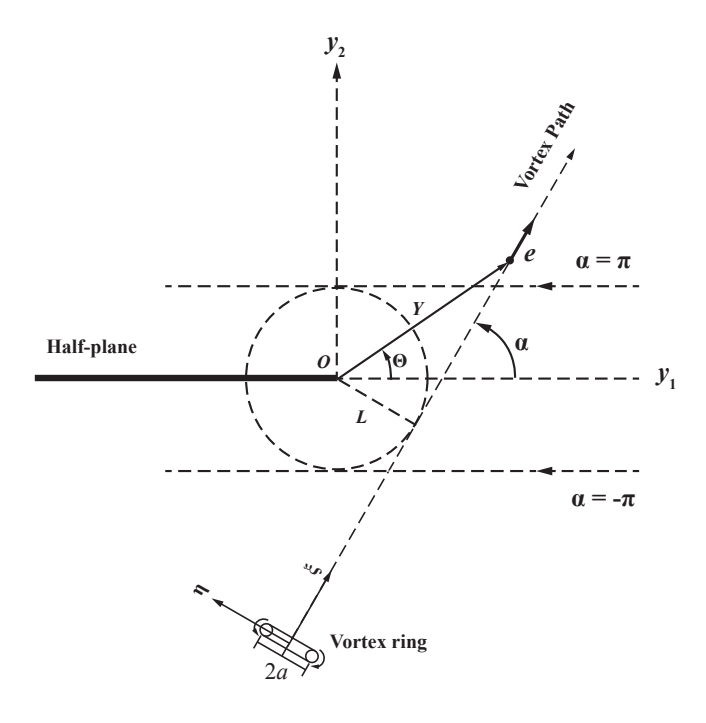


Fig. 2 Schematic of the vortex configuration and vortex path

C. Vortex ring model

Consider a thin-cored vortex ring, whose center moves in a plane perpendicular to the y_3 axis, as shown in Fig. 2. O is the coordinate origin located at the half-plane edge, and L is the nearest distance of the vortex ring path to the edge. It is assumed that L is larger than the vortex radius a such that the vortex does not collide with the edge. The normal to the plane of the vortex ring lies in the (y_1, y_2) -plane, and ξ axis denotes the vortex path direction. The η axis is taken to be perpendicular to ξ in the counterclockwise direction. The origin of the (ξ, η, y_3) coordinate system is located at the vortex center. The vorticity of the vortex ring is assumed to be concentrated in the circle of radius a with a small vortex core of radius δ ($\delta/a \ll 1$). The vorticity components in (ξ, η, y_3) -system are represented by

$$(0, -\Gamma\delta(\xi)\delta(\zeta - a)\sin\phi, \Gamma\delta(\xi)\delta(\zeta - a)\cos\phi), \tag{21}$$

where $\zeta = \sqrt{\eta^2 + y_3^2}$, Γ is the strength of vortex ring. ϕ is the azimuthal angle of the vortex center from the η axis, and ζ the radial coordinate in the (η, y_3) -plane. It is worth noting that this model setup is the same as that by Kambe *et al.* [12], which permits parametric comparisons against their analysis for a rigid edge.

1. Porous-rigid case

Substituting Eq. (21) in Eq. (15) yields,

$$p_{rp}\left(\mathbf{x},t+\frac{x}{c}\right) = \rho_0 \Gamma D_t^2 \int_0^{2\pi} F(\zeta = a, \xi = 0; \mathbf{C}(t)) a \cos\phi d\phi, \tag{22}$$

where C(t) represents the position of the vortex center at time t, and the dependence of F on x has been suppressed here for simplicity. Following the procedure by Kambe $et\ al.\ [12]$, F can be approximated by the two-term Taylor expansion with respect to η ,

$$F(\zeta = a, \xi = 0; \mathbf{C}) = F(\mathbf{C}) + \frac{\partial}{\partial \eta} F(\mathbf{C}) a \cos \phi, \tag{23}$$

since F is independent of ϕ . Then we have

$$\int_{0}^{2\pi} Fa\cos\phi d\phi = \pi a^{2} \frac{\partial}{\partial \eta} F(\mathbf{C}) = B_{rp} \pi a^{2} v_{n}(\mathbf{C})$$
(24)

where

$$v_n = \frac{\partial}{\partial \eta} \Psi_{\frac{1}{2}}(C) = \frac{\partial}{\partial \xi} \Phi_{\frac{1}{2}}(C), \tag{25}$$

$$B_{rp} = \frac{1}{2\pi^{\frac{3}{2}}c} \frac{\sin\theta_0 \sin\psi_0}{\mu^{\frac{1}{2}}x}.$$
 (26)

Thus, we find the acoustic pressure expression in the highly-porous parametric limit to be

$$p_{rp}\left(x,t+\frac{x}{c}\right) = \frac{\rho_0 \Gamma}{2\pi^{\frac{3}{2}}c} \frac{\sin\theta_0 \sin\psi_0}{\mu^{\frac{1}{2}}x} D_t^2 [\pi a^2 v_n(C)]. \tag{27}$$

Note that $\pi a^2 v_n$ is the volume flux of the hypothetical potential flow $\Phi_{\frac{1}{2}}$ passing through the vortex ring. It is now clear that the sound pressure has the directivity proportional to $\sin \theta_0 \sin \psi_0$, and the temporal profile of the pressure is found to be proportional to the acceleration of the volume flux through the vortex ring. The term $D_t^2[\pi a^2 v_n(C)]$ must now be evaluated to furnish scaling estimates of the acoustic emission.

Recalling that $D_t^2 v_n(C) = D_t[D_t v_n(C)]$, the evaluation of $D_t v_n(C)$ is now pursued. Suppose that the vortex ring moves rectilinearly with velocity Ue, where e is a unit vector with components $(\cos \alpha, \sin \alpha)$ in the (y_1, y_2) -plane (cf. Fig. 2) and the vortex path is sufficiently distant from the edge (L > a). This assumption of the rectilinear vortex motion has been shown to be valid by Kambe $et\ al$. [12] for the sound problem of a vortex ring near an impermeable-rigid plane. Following Kambe $et\ al$.'s method, the first derivative of v_n is

$$D_t v_n = U \boldsymbol{e} \cdot \nabla v_n(\boldsymbol{C}) = U(\boldsymbol{e} \cdot \nabla)^2 \Phi_{\frac{1}{2}}(\boldsymbol{Y}), \tag{28}$$

and

$$v_n(\mathbf{C}) = \frac{\partial}{\partial \xi} \Phi_{\frac{1}{2}}(\mathbf{Y}) = (\mathbf{e} \cdot \nabla)^2 \Phi_{\frac{1}{2}}(\mathbf{Y}). \tag{29}$$

It is convenient to introduce the complex variable $z = y_1 + iy_2 = Ye^{i\Theta}$, then we have

$$(\boldsymbol{e} \cdot \nabla)\Phi_{\frac{1}{2}} = \operatorname{Re}\left\{e^{\mathrm{i}\alpha}\frac{\mathrm{d}f}{\mathrm{d}z}\right\}, \quad f = \Phi_{\frac{1}{2}}(\boldsymbol{Y}) + \mathrm{i}\Psi_{\frac{1}{2}}(\boldsymbol{Y}) = -\mathrm{i}z^{\frac{1}{2}}. \tag{30}$$

Substituting $\Phi_{\frac{1}{2}}(Y) = Y^{\frac{1}{2}} \sin \frac{\theta}{2}$ into Eq. (30), we have

$$(\boldsymbol{e} \cdot \nabla)\Phi_{\frac{1}{2}}(\boldsymbol{Y}) = -\frac{1}{2}\boldsymbol{Y}^{-\frac{1}{2}}\sin\left(\frac{1}{2}\Theta - \alpha\right), \quad (\boldsymbol{e} \cdot \nabla)^{2}\Phi_{\frac{1}{2}}(\boldsymbol{Y}) = \frac{1}{4}\boldsymbol{Y}^{-\frac{3}{2}}\sin\left(\frac{3}{2}\Theta - 2\alpha\right). \tag{31}$$

Let the time origin to be the instant when the vortex ring is nearest to the edge with the distance Y = L. The vortex position at time t can then be represented by

$$(Y\cos\Theta, Y\sin\Theta) = (Ut\cos\alpha \pm L\sin\alpha, Ut\sin\alpha \mp L\cos\alpha),$$
 (32)

where the upper sign holds for $0 \le \alpha \le \pi$, and the lower sign holds for $0 \ge \alpha \ge -\pi$.

Normalizing the lengths and time by L and L/U, respectively, we have

$$D_t^2[\pi a^2 v_n(\mathbf{C})] = \frac{1}{4} \pi a^2 U^2 L^{-\frac{5}{2}} D_t \left[g(\bar{t}) \right], \tag{33}$$

where

$$g(\bar{t}) = r^{-\frac{3}{2}} \sin\left(\frac{3}{2}\Theta - 2\alpha\right),\tag{34}$$

$$r = \left(\overline{t}^2 + 1\right)^{\frac{1}{2}}, \quad \Theta = \tan^{-1}\left(\frac{\overline{t}\sin\alpha \mp \cos\alpha}{\overline{t}\cos\alpha \pm \sin\alpha}\right), \quad \overline{t} = \frac{U}{L}t. \tag{35}$$

The substitution of Eqs. (33), (34) and (35) into Eq. (27) yields the pressure,

$$p_{rp}\left(\mathbf{x},t+\frac{x}{c}\right) = \frac{a^2 \rho_0 \Gamma U^2}{8\pi^{\frac{1}{2}} c L^{\frac{5}{2}}} \frac{\sin \theta_0 \sin \psi_0}{\mu^{\frac{1}{2}} x} D_t \left[g\left(\overline{t}\right)\right],\tag{36}$$

where the velocity U of a vortex ring is determined by the well-known formula [17]

$$U = \frac{\Gamma}{4\pi a} \left(\ln \frac{8a}{\delta} - \frac{1}{4} \right). \tag{37}$$

From Eq. (36), the acoustic pressure for a rigid-porous edge scales as

$$p_{rp} \sim U^3 L^{-\frac{5}{2}}. (38)$$

The corresponding acoustic intensity Π_{rp} is given by the following formula [18]

$$\Pi_{rp} \sim \frac{p_{rp}^2}{\rho_0 c} \sim U^6 L^{-5},$$
 (39)

where from Eq. (36) the acoustic intensity has a directional dependence on $\sin^2 \theta_0$ for a given source angular position ψ_0 .

2. Impermeable-elastic case

Similarly, the pressure formula for the impermeable-elastic case is

$$p_e\left(x, t + \frac{x}{c}\right) = \frac{\mathrm{i}\rho_0 \Gamma}{2\pi^{\frac{3}{2}} c^{\frac{3}{2}}} \frac{\sin \theta_0 \sin \psi_0}{\epsilon^{\frac{1}{2}} x} D_t^{\frac{5}{2}} [\pi a^2 v_n(\mathbf{C})]. \tag{40}$$

From Eqs. (28) and (29), the second derivative of v_n is

$$D_t^2 v_n = (U \boldsymbol{e} \cdot \nabla)^2 v_n(\boldsymbol{C}) = U^2 (\boldsymbol{e} \cdot \nabla)^3 \Phi_{\frac{1}{2}}(\boldsymbol{Y}), \tag{41}$$

and from Eq. (31), we have

$$(\boldsymbol{e} \cdot \nabla)^3 \Phi_{\frac{1}{2}}(\boldsymbol{Y}) = -\frac{3}{8} \boldsymbol{Y}^{-\frac{5}{2}} \sin\left(\frac{5}{2}\Theta - 3\alpha\right). \tag{42}$$

Following the approach with Eq. (32) and choosing the same scaled length and time,

$$D_t^{\frac{5}{2}}[\pi a^2 v_n(\mathbf{C})] = -\frac{3}{8}\pi a^2 U^{\frac{5}{2}} L^{-3} D_t^{\frac{1}{2}}[m(\bar{t})], \qquad (43)$$

where

$$m\left(\overline{t}\right) = r^{-\frac{5}{2}}\sin\left(\frac{5}{2}\Theta - 3\alpha\right),\tag{44}$$

The substitution of Eqs. (43), (44) and (35) into Eq. (40) yields the pressure,

$$p_{e}\left(x,t+\frac{x}{c}\right) = -\frac{i3a^{2}\rho_{0}\Gamma U^{\frac{5}{2}}}{8\pi^{\frac{1}{2}}c^{\frac{3}{2}}L^{3}} \frac{\sin\theta_{0}\sin\psi_{0}}{\epsilon^{\frac{1}{2}}x} D_{t}^{\frac{1}{2}}\left[m\left(\bar{t}\right)\right]. \tag{45}$$

The corresponding acoustic pressure for an impermeable-elastic edge in Eq. (40) is proportional to

$$p_e \sim U^{\frac{7}{2}} L^{-3},$$
 (46)

and the acoustic power Π_e is

$$\Pi_e \sim \frac{p_e^2}{\rho_0 c} \sim U^7 L^{-6},$$
 (47)

and the directivity has the same $\sin^2 \theta_0$ dependence as the highly porous-rigid case.

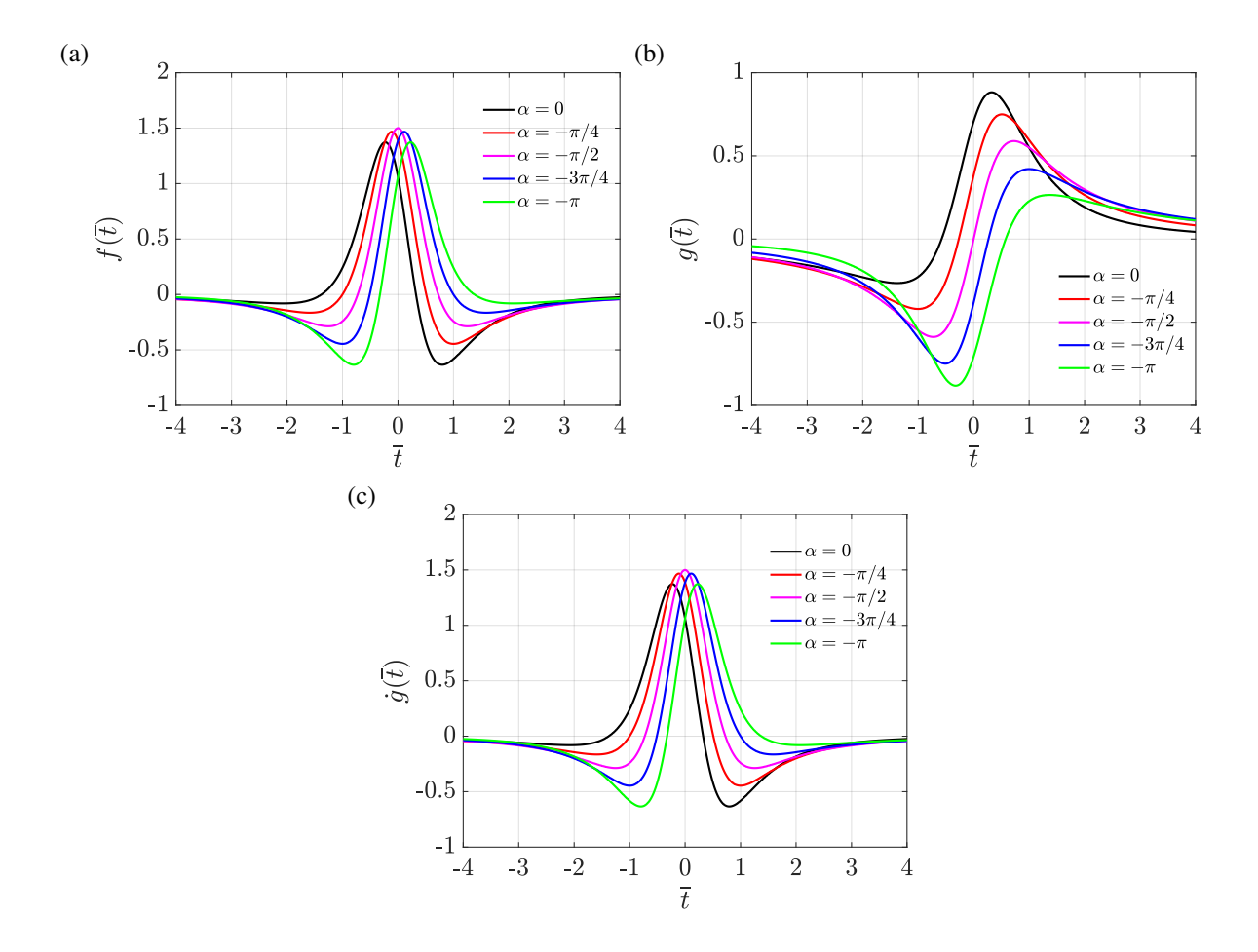


Fig. 3 Rigid-porous case: time histories of three functions $f(\bar{t})$, $g(\bar{t})$, and $\dot{g}(\bar{t})$ for five inclination angles α of the vortex path relative to the edge. $f(\bar{t}) = D_t[g(\bar{t})]$ is the dimensionless acoustic pressure and has the same behavior of $\dot{g}(\bar{t})$.

III. Results

In this section, the results for cases of porous edge and elastic edge are presented. The model setups for these edge conditions permit direct comparisons against previous results for a rigid edge setup by Kambe *et al.* [12].

A. Porous-rigid case

The time history of the far-field acoustic pressure scattered by a highly porous-rigid case in Eq. (36) is governed by

$$f\left(\overline{t}\right) = D_t \left[g\left(\overline{t}\right)\right] = \dot{g}\left(\overline{t}\right),\tag{48}$$

where the three functions $f(\bar{t})$, $g(\bar{t})$, and $\dot{g}(\bar{t})$ were plotted in Fig. 3 for five inclination angles α of the vortex path relative to the edge $(\alpha = 0, -\frac{1}{4}\pi, -\frac{1}{2}\pi, -\frac{3}{4}\pi, -\pi)$, as illustrated in Fig. 2. Note that the expressions of $g(\bar{t})$, $\dot{g}(\bar{t})$, and the selections of α are the same as that presented by Kambe *et al.* [12] for the convenience of comparisons between different cases. For the rigid case, the dimensionless acoustic pressure is the $\frac{1}{2}$ th derivative of $g(\bar{t})$, but for the porous case, the acoustic pressure is determined by the first derivative of $g(\bar{t})$ such that the curve of $f(\bar{t})$ is identical to that of $\dot{g}(\bar{t})$ (cf. Fig. 3 (a) (c)).

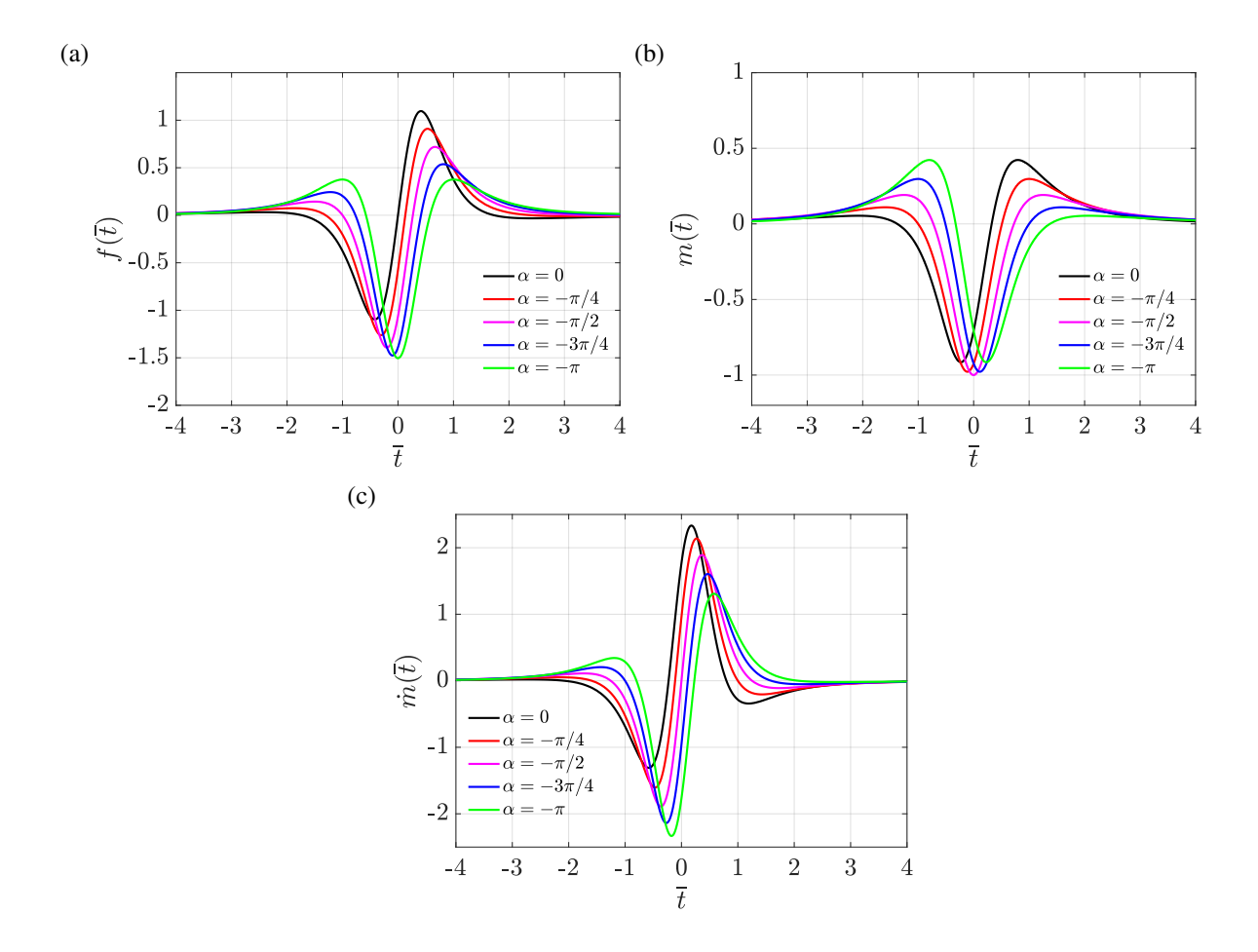


Fig. 4 Impermeable-elastic case: time histories of three functions $f(\bar{t})$, $m(\bar{t})$, and $\dot{m}(\bar{t})$ for five inclination angles α of the vortex path relative to the edge. $f(\bar{t}) = D_t^{\frac{1}{2}} \left[m(\bar{t}) \right]$ is the dimensionless acoustic pressure and shows an intermediate behavior between that of $m(\bar{t})$ and $\dot{m}(\bar{t})$.

B. Impermeable-elastic case

The corresponding time dependence of the acoustic pressure from an elastic edge with $k\epsilon^{-1/2} \ll 1$ is represented by

$$f\left(\overline{t}\right) = D_{t}^{\frac{1}{2}}\left[m\left(\overline{t}\right)\right] = \frac{1}{2\pi} \int_{-\infty}^{+\infty} (-\mathrm{i}\omega)^{\frac{1}{2}} \hat{m}(\omega) e^{-\mathrm{i}\omega t} d\omega = \int_{-\infty}^{t} \frac{\dot{m}(s)}{\left[\pi(t-s)\right]^{\frac{1}{2}}} ds,\tag{49}$$

where the three functions $f(\bar{t})$, $m(\bar{t})$, and $\dot{m}(\bar{t})$ were plotted in Fig. 4 for five inclination angles α of the vortex path relative to the edge $(\alpha = 0, -\frac{1}{4}\pi, -\frac{1}{2}\pi, -\frac{3}{4}\pi, -\pi)$. For the elastic case, the dimensionless acoustic pressure is the $\frac{1}{2}$ th derivative of $m(\bar{t})$, and shows an intermediate behavior between that of $m(\bar{t})$ and $\dot{m}(\bar{t})$.

It is worth noting that Kambe *et al.* [12] identified a symmetric acoustic pressure signal (proportional to $f(\bar{t})$) for a rigid, impermeable edge when $\alpha = 0$. However, the curves of $f(\bar{t})$ shown in Figs. 3 and 4 show that symmetric pressure signals occur for vortex path angles $\alpha = -\pi/2$ and $\alpha = -\pi$ for the porous case and the elastic case, respectively.

IV. Conclusions

An analytical framework is developed to estimate the far-field sound from a vortex ring passing near a rigid-porous or an impermeable-elastic edge. We adapts the works of Kambe *et al.* [12] for an impermeable-rigid edge condition, which permits a parametric check and direct comparisons on this analysis of different edge conditions. The time-domain Green's functions for the porous and elastic cases are developed in this work by extending the vortex-ring analysis

procedure by Kambe *et al.* [12] and integrating with it the asymptotic results for turbulence edge scattering for poroelastic plates by Jaworski and Peake [7].

In contrast to the U^5 acoustic power scaling law and cardioid directivity for turbulence and vortex sources near a rigid half plane, the present analysis identifies a U^6 scaling in a highly-porosity limit ($\mu/k \gg 1$) and a U^7 scaling for an elastic case under a specific limit of fluid loading condition ($k\epsilon^{-1/2} \ll 1$). Both cases yield a dipolar directivity of acoustic intensity, $\sin^2\theta_0$. Furthermore, new scalings on the minimum distance of the vortex ring from the edges are established, where L^{-5} and L^{-6} dependencies occur for the porous and elastic cases, respectively. The time-dependent component of the scattered field depends strongly on the orientation of the vortex path relative to the edge, where the particular impermeable, porous, and elastic cases examined each yield symmetric waveforms along different vortex-ring paths. This time-dependent information for the scattered pressure signal and the accompanying scaling trends of acoustic power on both the vortex ring speed U and offset distance from the edge L establish a basis for experimental validation of poroelastic-edge noise suppression in particular parametric limits.

Appendix

Apply the Fourier inversion formula in Eq. (6), equation (4) becomes

$$\left(\nabla^2 + k^2\right)\widehat{G}(x, y; k) = -\delta(x - y),\tag{50}$$

where k and ω are related by $k = \omega/c$ denote the wavenumber and the angular frequency, respectively.

The Green's function for the incident field is

$$\widehat{G}_0(x,y;k) = \frac{1}{4\pi |x-y|} e^{ik|x-y|}.$$
(51)

For observations at large distances $x \to \infty$, \widehat{G}_0 can be expressed asymptotically as

$$\widehat{G}_0(x, y; k) \sim A \exp[-ik(\widehat{x}_1 y_1 + \widehat{x}_2 y_2)],$$
 (52)

where

$$A = \frac{1}{4\pi x} \exp(ikx - ik\hat{x}_3 y_3),\tag{53}$$

and the direction of the observation point x is denoted by

$$\hat{x} = x/|x| = (\hat{x}_1, \hat{x}_2, \hat{x}_3),$$

$$\hat{x}_1 = \sin \psi_0 \cos \theta_0, \quad \hat{x}_2 = \sin \psi_0 \sin \theta_0, \quad \hat{x}_3 = \cos \psi_0.$$

From the result of the scattered field for a poroelastic edge by Jaworski and Peake [7], the corresponding Green's function for the scattered field can be derived,

$$\widehat{G}_{s}(x,y;k) = -\frac{1}{2} i Y^{1/2} \pi^{-3/2} B \sin \frac{\theta}{2} \frac{\exp \left[ikx - ik\cos \psi_{0} y_{3} + \frac{\pi}{4} i \right]}{r} \quad \text{as } Y \to 0,$$
 (54)

where $Y = (y_1^2 + y_2^2)^{\frac{1}{2}}$ and $k = \omega/c$. B is a variable that depends on k, the properties of the poroelastic edge, and the directivity of the incident field. The expression of B can be found in Eq. (4.16) by Jaworski and Peake [7]. Note that B must be determined numerically for a poroelastic edge setup, but can be determined numerically when considering the porous and elastic effects separately. Therefore, special attention is paid to the limiting cases of highly porous-rigid and impermeable-elastic edge conditions as determined parametrically by [7] in the following sections.

A. Porous-rigid case

For the highly porous-rigid case ($\delta \gg 1$, $\delta = \mu/k$), the variable B in Eq. (54) can be simplified as

$$B_{rp} = \frac{k \sin \theta_0 \sin \psi_0}{K_+(k \cos \theta_0 \sin \psi_0)} \sim \frac{k \sin \theta_0 \sin \psi_0}{\mu^{\frac{1}{2}} e^{\frac{i\pi}{4}}},\tag{55}$$

where $\mu = \alpha_H \overline{K}_R / R$ is a parameter determining the porous effects. Specifically, α_H is the open area fraction of the the surface with pores of nominal radius R, and $\overline{K}_R = 2K_R / (\pi R)$, where K_R is the Rayleigh conductivity of the pore [7]. The substitution of Eq. (55) into Eq. (54) lets the scattered field for the highly porous-rigid case be represented by

$$\widehat{G}_{s}(x,y;k) = \frac{1}{2\pi^{\frac{3}{2}}c}Y^{\frac{1}{2}}\sin\frac{\theta}{2}\frac{\sin\theta_{0}\sin\psi_{0}}{\mu^{\frac{1}{2}}x}(-i\omega)\exp(ikx - ik\cos\psi_{0}y_{3}).$$
 (56)

B. Impermeable-elastic case

For the impermeable-elastic case $(k\epsilon^{-1/2} \ll 1, \epsilon = \rho_0 k/(mk_B^2))$, the variable B in Eq. (54) can be simplified as

$$B_{e} = \frac{k \sin \theta_{0} \sin \psi_{0}}{K_{+}(k \cos \theta_{0} \sin \psi_{0})} \sim \frac{k^{\frac{3}{2}} \sin \theta_{0} \sin \psi_{0}}{\epsilon^{\frac{1}{2}}},$$
(57)

where ϵ is the intrinsic fluid loading parameter [7, 14, 16] that depends only on the properties of the structure and fluid, m is the plate mass, and k_B is the $in\ vacuo$ bending wavenumber.

Substitute Eq. (57) into Eq. (54), the scattered field for the impermeable-elastic case can be represented by

$$\widehat{G}_{s}(x,y;k) = \frac{i}{2\pi^{\frac{3}{2}}c^{\frac{3}{2}}}Y^{\frac{1}{2}}\sin\frac{\theta}{2}\frac{\sin\theta_{0}\sin\psi_{0}}{\epsilon^{\frac{1}{2}}x}(-i\omega)^{\frac{3}{2}}\exp(ikx - ik\cos\psi_{0}y_{3}).$$
 (58)

Acknowledgment

This work was supported by the National Science Foundation under awards 1805692, monitored by Dr. Ronald Joslin.

References

- [1] Lighthill, M. J., "On sound generated aerodynamically I. General theory," *Proceedings of the Royal Society of London A*, Vol. 211, No. 1107, 1952, pp. 564–587.
- [2] Curle, N., "The influence of solid boundaries upon aerodynamic sound," *Proceedings of the Royal Society of London A*, Vol. 231, No. 1187, 1955, pp. 505–514.
- [3] Ffowcs Williams, J., and Hall, L., "Aerodynamic sound generation by turbulent flow in the vicinity of a scattering half plane," *Journal of Fluid Mechanics*, Vol. 40, No. 4, 1970, pp. 657–670.
- [4] Crighton, D., and Leppington, F., "Scattering of aerodynamic noise by a semi-infinite compliant plate," *Journal of Fluid Mechanics*, Vol. 43, No. 4, 1970, pp. 721–736.
- [5] Cavalieri, A., Wolf, W., and Jaworski, J., "Numerical solution of acoustic scattering by finite perforated elastic plates," Proceedings of the Royal Society of London A, Vol. 472, No. 2188, 2016, p. 20150767.
- [6] Howe, M. S., "Structural and acoustic noise produced by turbulent flow over an elastic trailing edge," *Proceedings of the Royal Society of London A*, Vol. 442, No. 1916, 1993, pp. 533–554.
- [7] Jaworski, J. W., and Peake, N., "Aerodynamic noise from a poroelastic edge with implications for the silent flight of owls," *Journal of Fluid Mechanics*, Vol. 723, 2013, pp. 456–479.
- [8] Howe, M. S., "On the generation of sound by turbulent boundary layer flow over a rough wall," *Proceedings of the Royal Society of London A*, Vol. 395, No. 1809, 1984, pp. 247–263.
- [9] Devenport, W., Alexander, N., Glegg, S., and Wang, M., "The sound of flow over rigid walls," *Annual Review of Fluid Mechanics*, Vol. 50, 2018, pp. 435–458.
- [10] Glegg, S., and Devenport, W., "The far-field sound from rough-wall boundary layers," Proceedings of the Royal Society of London A, Vol. 465, No. 2106, 2009, pp. 1717–1734.
- [11] Crighton, D. G., "Radiation from vortex filament motion near a half plane," *Journal of Fluid Mechanics*, Vol. 51, No. 2, 1972, pp. 357–362.

- [12] Kambe, T., Minota, T., and Ikushima, Y., "Acoustic wave emitted by a vortex ring passing near the edge of a half-plane," *Journal of Fluid Mechanics*, Vol. 155, 1985, pp. 77–103.
- [13] Howe, M. S., "Contributions to the theory of aerodynamic sound, with application to excess jet noise and the theory of the flute," *Journal of Fluid Mechanics*, Vol. 71, No. 4, 1975, pp. 625–673.
- [14] Howe, M. S., Acoustics of fluid-structure interactions, Cambridge University Press, 1998.
- [15] Rayleigh, L., The theory of sound, Vol. 2, Dover, 1945.
- [16] Crighton, D. G., and Innes, D., "The modes, resonances and forced response of elastic structures under heavy fluid loading," Philosophical Transactions of the Royal Society of London A, Vol. 312, No. 1521, 1984, pp. 295–341.
- [17] Lamb, H., Hydrodynamics, Cambridge University Press, 1993.
- [18] Howe, M. S., Theory of vortex sound, Vol. 33, Cambridge University Press, 2003.